Finite Buffer Queuing Delay Performance in the Low Earth Orbit Land Mobile Satellite Channel

Néstor J. Hernández Marcano*, Luis Diez†, Ramon Agüero†, Rune Hylsberg Jacobsen*
*Department of Electrical and Computer Engineering, Aarhus University, Aarhus, Denmark. { nh | rhj}@ece.au.dk
†Communications Engineering Department, Universidad de Cantabria, Santander, Spain. { ldiez | ramon }@tlmat.unican.es

***Abstract*—Low Earth Orbit (LEO) satellite constellations have been identified for new massive access networks, as a complement to traditional cellular ones, due to their native ubiquity. Despite being a feasible alternative, such networks still raise questions on their performance, in particular regarding the delay and queuing management under realistic channels. In this work, we study the queuing delay of a single satellite-to-ground link, considering a Land Mobile Satellite (LMS) channel in LEO with finite buffer lengths. We analyze the trade-off between delay and packet loss probability, using a novel model based on Markov chains, which we assess and extend with an extensive analysis carried out by means of system level simulation. The developed tools capture with accuracy the queuing delay statistical behavior in the S and Ka frequency bands, where LEO communications are planned to be deployed. Our results show that we can use short buffers to ensure less than 5-10% packet loss, with tolerable delays in such bands.**

***Index Terms*—queuing, delay, loss probability, performance, LMS channel, LEO**

I. Introduction

Future terrestrial networks will exhibit an increasing difficulty to deal with eventual capacity bottlenecks given the more common use cases of Internet of Things (IoT) and Machine Type Communications (MTC). In this context, Non-Terrestrial Networks (NTN) [1] and, in particular, LEO satellite communications (in the so-called *NewSpace* era), will play a fundamental role to provide access and coverage where conventional networks fail to reach remote areas. Thus, maritime asset/vessel tracking, airplane connectivity, and remote IoT data aggregation appear as potential applications. LEO constellation and terrestrial network integration is being considered by cellular standardization bodies, since Release 15 from the Third Generation Partnership Project (3GPP) for 5G and 6G [2]. Such constellations rely on several spacecrafts for close-to-global coverage in different orbital planes, where they pose new questions on queuing delays within their links to ground. In this sense, existing works usually overlook limitations in buffer size of queuing systems under real channel conditions, limiting their analysis to legacy $M/M/1$ systems. In this work, we study the queuing delay of a *single* satellite-to-ground link using the LMS model discussed in [3], differing from the terrestrial case, which considers realistic satellite channel states as: Line of Sight (LoS), mid-shadowing or deep-shadowing. We develop a Markov chain analysis that includes finite buffer lengths, where packets might thus be dropped, bringing together the effects from both the shadowing conditions of the LMS channel and finite buffer queues. The proposed model is, to our best knowledge, the first attempt at capturing the trade-off between delay and queuing loss probability that might be exploited in the design of LEO networks.

In particular, our contributions are: (i) we provide a theoretical model for the LMS channel comprising both finite-length buffers and channel states, based on a bi-dimensional Markov chain, which allows studying the trade-off between delay and loss probability; (ii) we validate the proposed Markovian model with a system simulator in C++, allowing us to conduct a queuing delay distribution performance assessment. We consider various configurations of LEO frequency bands, buffer lengths, and traffic loads. The work is an extension of the one presented in [4], where we assumed infinite buffer lengths. Assuming finite buffers does not only require a new approach to solve the corresponding Quasi-Birth-Death (QBD), but it also yields a new set of results, where the loss probability can be actually studied as a performance indicator.

Our work is structured as follows. Section II reviews the state-of-the-art, allowing us to position the model proposed in this paper and depicted in Section III, which also discusses how it can be solved, exploiting Matrix Geometric techniques. Section IV validates the model, by means of an extensive simulation-based measurement campaign, carried out over an event-driven simulator, which is also used to broaden the analysis. Finally, Section V concludes the paper, identifying aspects that will be tackled in our future work.

II. State-of-the-Art Review

Although the LMS channel has been studied previously, the literature around different queuing models for the LEO LMS downlink jointly is scarce. Chen *et al.* used in [5] a discrete Markov chain to analyze delay in Automatic Repeat Request (ARQ) schemes. They assumed a time-slotted channel to study the impact of finite buffer lengths. On the other hand, Hermenier *et al.* proposed in [6] another Markov chain to model delay distributions for a rather specific scenario. Such models do not consider the LMS channel and depend on fixed delay distributions, where our proposed model could be adapted to different link characteristics. Past works have proposed revisions of the LMS channel. The works in [7] and [8] used different physical layer parameters for lesser channel states, but do not include their queuing effects. Our novel model allows to study the queuing delay/loss probability trade-off from the channel impact on the transmitter buffer. The queuing delay of a LEO

optical constellation is reviewed in [9], where contiguous Inter-Satellite Links (ISLs) between two Ground Stations (GSs) are studied to obtain an average queuing delay with Poisson-distributed traffic, infinite buffer lengths, and ideal channels. More recently, intermittent satellite links in LEO / Medium Earth Orbit (MEO) constellations are discussed in [10], under two channel status: working or vacation periods. It uses the Laplace-method to focus on average system performance, and do not consider finite buffer lengths. Regarding finite buffer lengths, the work in [11] considers traffic system simulations for buffer sizes avoiding bufferbloat, in the average queuing delay of Geostationary Orbit (GEO) / MEO with Transmission Control Protocol (TCP). However, the authors do not consider time-varying channels, since it focuses on the packet loss in the TCP data transfer period, rather than the channel state. Differentiating from all prior works, we proposed a queuing model for the LMS channel with infinite buffers in [4]. We now incorporate the finite buffer analysis of queues under LMS states for *S* and *Ka* bands, being representative of telemetry and mission data. We evaluate the trade-off between delay and loss probability aiming to serve as a design tool for ideal buffer lengths in future scenarios. We compute not only the analytical mean trends, but the complete delay distribution which can be exploited to design more appropriate reliable services.

III. System Model

We model the satellite-to-ground LMS link with the two-dimensional Markov chain shown in Figure 1. Packets arrive according to a Poisson process of rate λ. Packets are transmitted at different rates, depending on a generic fading channel status, between the satellite and the ground station.

A. Channel States, Transition Probabilities & Dwell Times

For the LMS channel, the channel states are: LoS, mid-shadowing, and deep-shadowing (see Figure 1). Table I enumerates the symbols are used in the paper. The service rate for each link status, μ_k can be calculated as $\mu_k = \frac{R_k}{\ell}$ where ℓ is the average packet length, and R_k is the transmission rate when the channel is in status k. We consider $\mu_{los} > \mu_{ms} > \mu_{ds} \geq 0$ to keep connectivity, whenever possible, under more stringent channel states.

The previous states are the three channel conditions that are identified by Fontan *et al.* [3], and they correspond to the rows in the Markov chain, while the number of packets in the system (either being transmitted, or in the interface buffer) are captured by the various columns. Hence, we can define all the states in the system as a tuple (i, j), where i is the number of packets in the system, and j represents the current channel status: 0 for deep-shadowing, 1 for mid-shadowing, and 2 for LoS conditions. Rightwards transitions (from (i, j) to $(i + 1, j)$) correspond to the arrival of a new packet, while leftwards transitions (from (i, j) to $(i - 1, j)$) reflect that a packet has been completely transmitted. We assume that the buffer has a maximum capacity of b packets. Hence, if a packet arrives when the system is at a $(b+1, j)$ state, i.e. one packet is being transmitted and b are waiting at the buffer (chain rightmost column), it will be lost. Based on the matrices that are given in [3], we can establish the average sojourn time at each channel status. Fontan *et al.* define a discrete Markov chain, with three different states to mimic the behavior of the LMS channel. The transitions between them are established by the following matrix, where l corresponds to LoS, m to mid-shadowing, and d to deep-shadowing conditions:

$$\mathcal{P} = \begin{pmatrix} p_{ll} & p_{lm} & p_{ld} \\ p_{ml} & p_{mm} & p_{md} \\ p_{dl} & p_{dm} & p_{dd} \end{pmatrix} \tag{1}$$

From (1) and assuming a certain slot time δ, we can derive the average dwell time at each of the channel states. We use the corresponding continuous transitions in the proposed Markov chain. To do so we use the geometric random variables that correspond to the number of contiguous slots at a particular channel status to yield the average time at each of them as follows:

$$\zeta_{\text{los}} = \frac{\delta}{1 - p_{ll}}, \quad \zeta_{\text{ms}} = \frac{\delta}{1 - p_{mm}}, \quad \zeta_{\text{ds}} = \frac{\delta}{1 - p_{dd}} \tag{2}$$

When the channel leaves a certain state, it can shift to one of the two other situations. The corresponding probabilities (α_{ij}) and so the transition rates (ξ_{ij}) can be also obtained from (1). If the current status is LoS for example, we have:

$$\alpha_{lm} = \frac{p_{lm}}{1 - p_{ll}}, \ \alpha_{ld} = \frac{p_{ld}}{1 - p_{ll}}; \ \xi_{\text{lm}} = \alpha_{lm}\zeta_{\text{los}}^{-1}, \ \xi_{\text{ld}} = \alpha_{ld}\zeta_{\text{los}}^{-1} \tag{3}$$

Which leads to a transition rate (dwell time inverse): $\zeta_{\text{los}}^{-1} = \xi_{lm} + \xi_{ld}$. The corresponding transitions from the two other channel status (mid-shadowing and deep-shadowing) are similarly obtained. This transition rates are represented in the Markov chain of Figure 1 by the vertical lines between states belonging to the same column.

TABLE I: Model variables and symbols

λ	Packet arrival rate
μ_k	Service rate of the k LMS state, $k = \{\text{los}, \text{ms}, \text{ds}\}$
b	Buffer length
p_{kj}	Transition probability between LMS states k and j $j, k = \{1\ (\text{los}), \text{m}\ (\text{ms}), \text{d}\ (\text{ds})\}$
δ	Time slot duration before possible channel state transitions
ζ_k	Dwell time at channel state k, $k = \{\text{los}, \text{ms}, \text{ds}\}$
α_{kj}	Probability of going to state j after leaving k $j, k = \{1\ (\text{los}), \text{m}\ (\text{ms}), \text{d}\ (\text{ds})\}$ and $k \neq j$
ξ_{kj}	Transition rate between channel states k and j $\xi_{kj} = \tau_k^{-1} \cdot \alpha_{kj}, \ k, j = \{1\ (\text{los}), \text{m}\ (\text{ms}), \text{d}\ (\text{ds})\}, \ k \neq j$
$\pi_i(j)$	Probability of state (i, j), $j = \{2\ (\text{los}), 1\ (\text{ms}), \ 0\ (\text{ds})\}$
π_i	Column vector: $[\pi_i(0)\ \pi_i(1)\ \pi_i(2)]^\intercal$
Q	Infinitesimal matrix of the QBD process
F	Forward transition matrix
B	Backward transition matrix
L, L_0, L_{b+1}	State transition matrices within the same level
$E[n]$	Mean number of packets at the LMS link
$E[\tau]$	Mean delay for the LMS links
$\mathcal{P}_{\text{loss}}$	Loss probability

B. Queuing Delay & Loss Probability Analysis

The model is analyzed as a QBD, due to the process matrix block structure. For the queuing delay and loss probability of

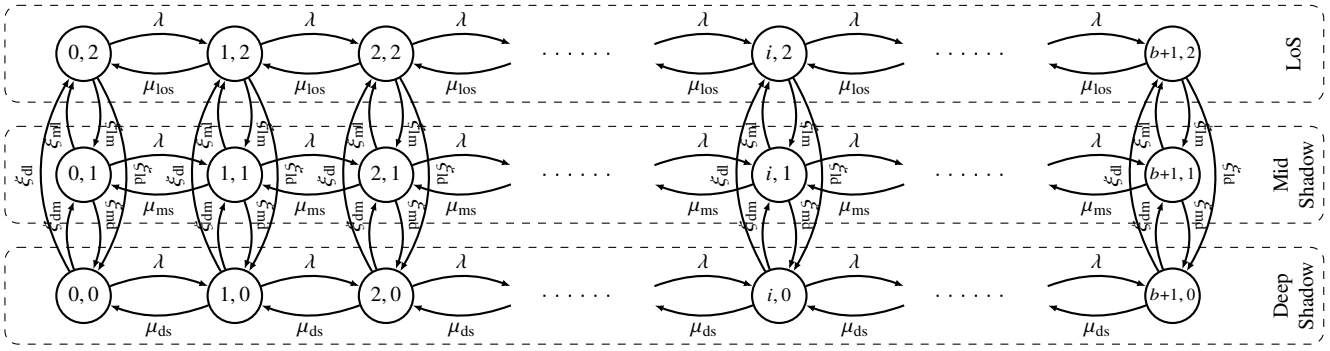

Fig. 1: Markov-chain model for the LMS link in the finite buffer regime.

the LMS model, we exploit the Matrix Geometric Method, as in [4], but now adapted to compute the stationary distribution in a finite buffer regime. The method is thoroughly discussed by Neuts [12] and Hajek [13]. We first define Q, the infinitesimal generator matrix of the QBD process:

$$Q = \begin{pmatrix} L_0 & F & 0 & 0 & \cdots & 0 & 0 & 0 & 0 \\ B & L & F & 0 & \cdots & 0 & 0 & 0 & 0 \\ 0 & B & L & F & \cdots & 0 & 0 & 0 & 0 \\ \vdots & & \ddots & & \ddots & & \ddots & & \vdots \\ 0 & 0 & 0 & 0 & \cdots & B & L & F & 0 \\ 0 & 0 & 0 & 0 & \cdots & 0 & B & L & F \\ 0 & 0 & 0 & 0 & \cdots & 0 & 0 & B & L_{b+1} \end{pmatrix}, \quad (4)$$

where L_0, F, B, L, L_{b+1} are 3×3 matrices. The overall dimension of Q is: $3(b+2)\times3(b+2)$. F and B are given in (5). The forward matrix (F) is the identity matrix multiplied by the incoming packet rate (λ), while the backwards matrix (B) is a diagonal matrix, whose elements correspond to the service rates of the three channel status, and both indicate how packets arrive or are processed.

$$F = \begin{pmatrix} \lambda & 0 & 0 \\ 0 & \lambda & 0 \\ 0 & 0 & \lambda \end{pmatrix} \quad ; \quad B = \begin{pmatrix} \mu_{\text{los}} & 0 & 0 \\ 0 & \mu_{\text{ms}} & 0 \\ 0 & 0 & \mu_{\text{ds}} \end{pmatrix} \quad (5)$$

On the other hand, L is defined as follows:

$$L = \begin{pmatrix} -(\lambda+\mu_{\text{los}}+\zeta_{\text{los}}^{-1}) & \xi_{\text{lm}} & \xi_{\text{ld}} \\ \xi_{\text{ml}} & -(\lambda+\mu_{\text{ms}}+\zeta_{\text{ms}}^{-1}) & \xi_{\text{md}} \\ \xi_{\text{dl}} & \xi_{\text{dm}} & -(\lambda+\mu_{\text{ds}}+\zeta_{\text{ds}}^{-1}) \end{pmatrix} \quad (6)$$

while $L_0 = L+B$, and $L_{b+1} = L+F$. The stationary distribution of the system is given by $\mathbf{\Pi} = [\pi_0\, \pi_1 \ldots \pi_{b+1}]$, where π_i is a column vector of three components $j = 0, 1, 2$, so that $\pi_i(j)$ corresponds to the probability of having i packets in the system, when the LMS is status j. In order to find such distribution, we first need to establish the intermediate matrices V and $\widetilde{V}$ [13, Theorem 1]:

$$V = -VFVBL^{-1} - L^{-1} \; ; \; \widetilde{V} = -\widetilde{V}B\widetilde{V}FL^{-1} - L^{-1} \quad (7)$$

Since there is not a closed solution for V and $\widetilde{V}$, we use an iterative method to obtain them. Such matrices are used to derive the first and last rows of the fundamental matrix, $\mathcal{N}$ of the QBD process [13, Theorem 4], which are shown in (8).

Then, using (8), we can finally build $\mathcal{M}$ [13, Theorem 5]:

$$\mathcal{M} = \begin{pmatrix} L_0 + F\mathcal{N}_{1,1}B & F\mathcal{N}_{1,b}F \\ B\mathcal{N}_{b,1}B & L_{b+1} + B\mathcal{N}_{b,b}F \end{pmatrix} \quad (9)$$

We then obtain $[\mathbf{x}_0\, \mathbf{x}_{b+1}]$, as the left eigenvector (with a eigenvalue of 1) of $\mathcal{M}$. Then [13, Theorem 5]:

$$\mathbf{x}_k^\intercal = \mathbf{x}_0^\intercal F N_{1,k} + \mathbf{x}_{b+1}^\intercal B N_{b,k} \quad k = 1, \ldots, b \quad (10)$$

The stationary distribution of the QBD process is given by:

$$\mathbf{\Pi} = \frac{1}{C}\left[\mathbf{x}_0\, \mathbf{x}_1 \ldots \mathbf{x}_{b+1}\right], \quad \text{where } C = \left(\sum_{i=0}^{b+1} \|\mathbf{x}_i\|_1\right)^{-1} \quad (11)$$

is a normalization constant. Once we compute the probabilities of all states, we can use them to analyze the performance of the LMS link. We use the mean number of packets in the system, $E[n]$, as well as the mean served packet rate, $E[\lambda]$, to find the mean queuing delay $E[\tau]$ by Little's Law:

$$E[\tau] = \frac{E[n]}{E[\lambda]} = \frac{\sum_{i=0}^{b+1} i\|\pi_i\|_1}{\lambda \sum_{i=0}^{b} \|\pi_i\|_1} \quad (12)$$

We can also exploit the Poisson-arrivals-see-time-averages (PASTA) property to find $\mathcal{P}_{\text{loss}} = \|\pi_{b+1}\|_1$.

IV. Results

In this section, we validate the proposed model exploiting an event-driven simulator [14] developed from scratch in C++. This tool considers three different events: (1) arrival of a new packet; (2) transmission of a packet; and (3) change of channel status. Each of them are handled according to the features of the LMS link, with traces kept to enable the performance analysis. Further, the simulator is used to not only validate the model, but also investigate the delay variability performance, since it might be a performance indicator for certain types of services. We study the performance of two LMS channels, for the *S* and *Ka* bands, each with different service rates for the *deep-shadowing* status. Table II depicts the configurations we used in all experiments. The service rates for the bands correspond to an average packet length of ℓ = 125 `Bytes`

$$\begin{pmatrix} \mathcal{N}_{1,1} & \cdots & \mathcal{N}_{1,b} \\ \mathcal{N}_{b,1} & \cdots & \mathcal{N}_{b,b} \end{pmatrix} = -\begin{pmatrix} L+FVB & -(FVB)^b B \\ -(B\widetilde{V})^b F & B\widetilde{V}F+L \end{pmatrix}^{-1} \cdot \begin{pmatrix} I & FV & \cdots & (FV)^{b-2} & (FV)^{b-1} \\ (B\widetilde{V})^{b-1} & (B\widetilde{V})^{b-2} & \cdots & B\widetilde{V} & I \end{pmatrix} \tag{8}$$

TABLE II: Scenario setup

S band LMS parameters from [3, Table III]	
$[\mu_{\text{los}}, \mu_{\text{ms}}, \mu_{\text{ds}}]$	[5, 2.5, 1]; [5, 2.5, 0] pkt/ms
LMS transition matrix	$\mathcal{P} = \begin{pmatrix} 0.8177 & 0.1715 & 0.0108 \\ 0.1544 & 0.7997 & 0.0459 \\ 0.1400 & 0.1433 & 0.7167 \end{pmatrix}$
LMS probabilities	[0.4545 0.4545 0.0910]
δ	100 ms
***Ka* band** LMS parameters from [3, Table XVII]	
$[\mu_{\text{los}}, \mu_{\text{ms}}, \mu_{\text{ds}}]$	[100, 50, 20]; [100, 50, 0] pkt/ms
LMS transition matrix	$\mathcal{P} = \begin{pmatrix} 0.6048 & 0.3648 & 0.0268 \\ 0.0473 & 0.8630 & 0.0897 \\ 0.0420 & 0.5579 & 0.4001 \end{pmatrix}$
LMS probabilities	[0.1055 0.7741 0.1204]
δ	100 ms

and (LoS) capacities of 5 `Mbps` and 100 `Mbps`, for *S* and *Ka* bands, respectively. The mid-shadowing is 50% with respect to the capacity and the deep-shadowing is either 20% of the capacity or zero (no connection).

A. Channel State Probability Distributions

Figure 2 compares the theoretical probabilities with the values obtained with the simulator for a particular system configuration. Each bin corresponds to the probability of having n packets in the system, from $n = 0$ to $b + 1$, where b is the buffer length (in this case, $b = 15$). In addition, we use colors to differentiate the current LMS channel status: dark green for *LoS*, pale green for *mid-shadowing*, and red for *deep-shadowing*. Left darker bars correspond to the values obtained with the proposed model, while paler right bars are results obtained with the simulator. We see that there is an almost ideal match with the simulation results , thus validating both the proposed model and the simulator. Figure 3 shows the values obtained using the proposed model for the *S* band. We see that the LMS channel probabilities do not depend on the particular configuration (buffer length, service rates, or traffic load), and match the theoretical values (see Table II). More interestingly, the figure yields that *deep-shadowing* is only relevant when the buffer is almost full. Similarly, the *LoS* case corresponds when there are fewer packets in the system. Thus, when the system is able to drain packets faster (*LoS*), the buffer gets empty, and when entering the *deep-shadowing* situation, especially when μ_{ds} equals 0, packets tend to fill the buffer.

B. Average Queuing Delay

Figure 4a shows the evolution of the average delay when we increase the incoming traffic rate for the *S* band. Solid and dashed lines are the results obtained with the proposed model, for buffer lengths $b = 7$, and $b = 15$, respectively. Markers correspond to the results obtained with the simulator, averaging 100 independent runs, with 10^6 packets sent each.

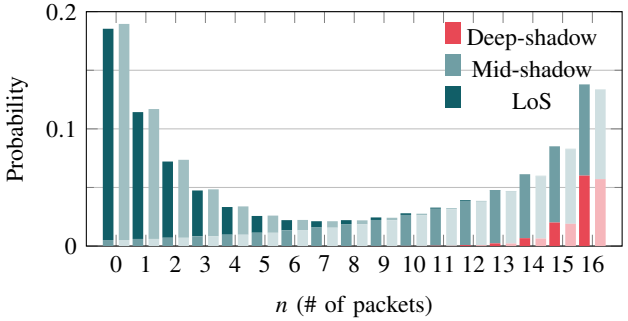

Fig. 2: State probabilities with the proposed model (left dark bars) and obtained with the simulator (right pale bars). Buffer length is $b = 15$, $\mu_{\text{ds}} = 1$ pkt/ms, and $\lambda = 3$ pkt/ms.

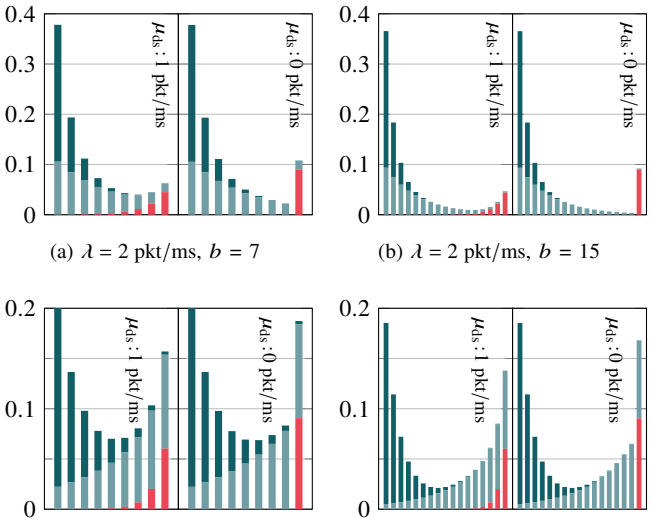

(a) $\lambda = 2$ pkt/ms, $b = 7$ (b) $\lambda = 2$ pkt/ms, $b = 15$

(c) $\lambda = 3$ pkt/ms, $b = 7$ (d) $\lambda = 3$ pkt/ms, $b = 15$

Fig. 3: State probabilities. *S* band. Dark green correspond to *LoS* condition, pale green with *mid-shadowing*, and red with *deep-shadowing*. In all graphs, x-axis corresponds to the number of packets at the system, n.

Again, there is an almost perfect match between the two approaches. The delay increases with λ, but there is an interesting effect, when μ_{ds} equals 0. Under this circumstance, and for low λ, the delay is rather large. This is due to the fact that there might be packets arriving when the channel is in the deep-shadowing status, and cannot be transmitted. Since the load is low, they are not likely to be lost, and they need to wait at the buffer until the channel leaves the deep-shadowing status. When λ increases, packets arriving when the system is at such state are likely to be lost. On the other hand, we can also see a change on the delay tendency when λ equals the service rate of either *mid-shadowing* (2.5 pkt/ms) or *deep-shadowing* (1 pkt/ms for the green lines) states, especially when the buffer length is longer. As can be seen in Figure 4b,

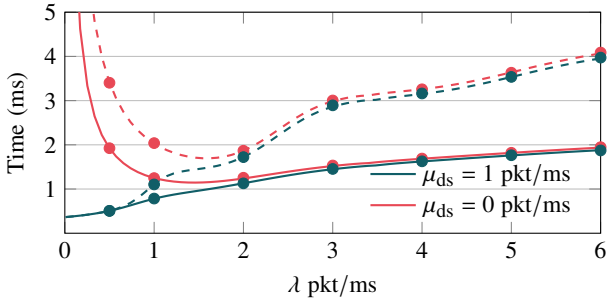

(a) *S* band

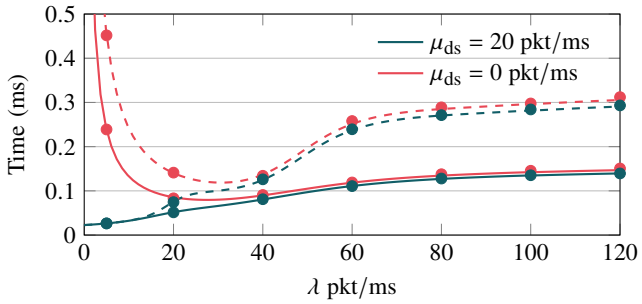

(b) *Ka* band

Fig. 4: Average delay in LMS channel. Solid and dashed lines are for buffer lengths of $b = 7$ and $b = 15$, respectively, obtained with the proposed model. Markers correspond to the results obtained with the simulator.

the behavior for the *Ka* band is similar, although the delay stabilizes faster. Again, simulation and theoretical results are almost alike.

C. Finite Buffer Queuing Delay Distribution

After validating the simulator, we can broaden the analysis for the delay variability. Figure 5 presents such variability, since there might be some services (with real-time requirements) where it is relevant to keep such dispersion (*jitter*) within reasonable values. We run a long experiment per configuration (with 10^6 packets) and we use box plots with whiskers to characterize the distribution of the corresponding delays for the *S* band.The limits of the boxes correspond to 0.75− and 0.25−percentiles, while the whisker limits are 0.95− and 0.05−percentiles. The horizontal line within the box is the median (0.5−percentile), and the circles correspond to the average value that was discussed in Figure 4a. We can see that the variability of the delay does not heavily increase (this is a consequence of having a limited buffer), and it is kept constant for λ greater than 3 pkt/ms. It is interesting to mention that the average delay for low λ, and $\mu_{ds} = 0$ pkt/ms is above the 0.95-percentile, due to several outliers from packet arrivals at the system with a *deep-shadowing* channel state, which need to be kept in the buffer until processed, as mentioned earlier.

D. Buffer Loss Probability & Delay-Loss Prob. Trade-off

Figure 6 shows the packet loss probability in the *S* band. We see again good model/simulation match, and a negligible

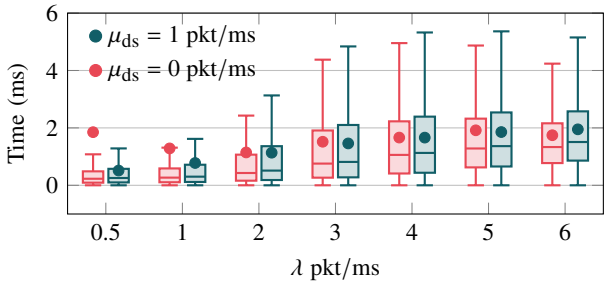

(a) $b = 7$

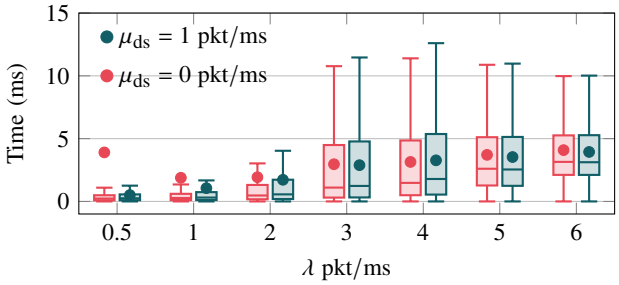

(b) $b = 15$

Fig. 5: Box plot of delay vs. traffic load λ. *S* band.

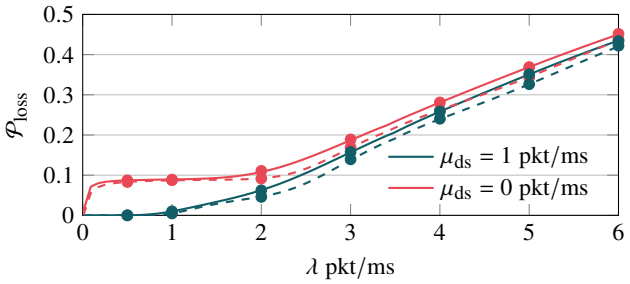

Fig. 6: Loss probability. *S* band. Solid and dashed lines are for buffer lengths of $b = 7$ and $b = 15$, respectively, obtained with the proposed model. Markers correspond to the results obtained with the simulator.

difference on the probability when increasing the buffer length. This is due to packets being processed regardless of the buffer size, and the packet loss being dependent mostly on traffic and channel states. In addition, for λ greater than 3 pkt/ms, the loss probabilities for the two *deep-shadowing* configurations are rather similar as well, and the benefit of having a service rate of $\mu_{ds} = 1$ pkt/ms is just relevant for low packet incoming rates. In this sense, when $\mu_{ds} = 0$ pkt/ms, there exists a minimum loss rate (≈ 0.1), which cannot be avoided, regardless of the traffic load. In any case, the loss probabilities might reach rather high values. Results for the *Ka* band were similar, but are omitted due to space constraints. Previous results have shown that, while the delay shows a slow increasing trend as λ gets higher, the loss probability grows at a much quicker pace. In order to better understand the trade-off between these two performance indicators, we used a different configuration, where we kept the traffic load (λ), and we increased the buffer length. We established the delay and the loss probability for each b value, and we plot the

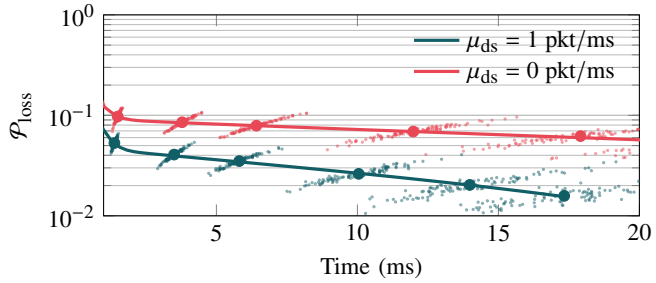

(a) *S* band. $\lambda = 2$ pkt/ms

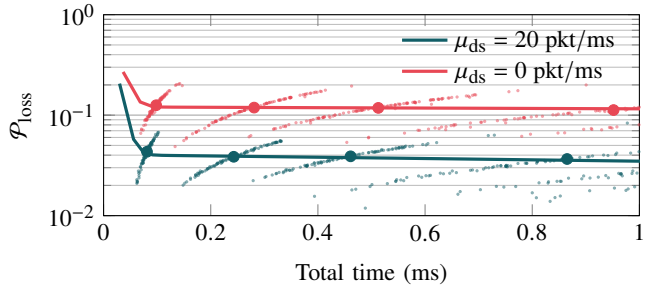

(b) *Ka* band. $\lambda = 30$ pkt/ms

Fig. 7: Loss probability Vs. Delay. Operation regions as we increase buffer length. Solid lines are theoretical results. Small markers are the performance observed in a single experiment, while big markers correspond to the average performance yielded by the simulator.

corresponding operation region. Figure 7 shows the results that were observed for the two bands. The solid lines correspond to the results yielded by the theoretical model, while we have use a scatter plot to represent the delay/loss probability tuples for the 100 independent simulation runs (for each buffer length, b), as well as the corresponding average value. The figure again shows the match between analytical values and the results obtained with the simulator. We can clearly observe the behavior that was seen with the previous experiments. After an initial sharp decrease of the loss probability, with a minor penalty in terms of delay, the figure yields that increasing the buffer length would bring a slight improvement of the loss probability, but at the cost of suffering a much longer delay. On the other hand, the variability of the system performance increases for longer buffer lengths, in particular in terms of the delay, as can be seen with the higher dispersion of the corresponding scatter plots.

V. Conclusions

The paper proposes a novel model through queuing theory to study the impact of finite buffers in the LMS channel, as a tool to properly estimate their size in LEO communications, and considering the trade-off between delay and packet loss probability. QBD theory has been exploited to yield the average performance. Then, a public event-driven C++ simulator [14] has been used to assess the proposed model, and we afterwards exploited it to study the delay variability performance. The results evince that increasing buffer lengths do not always lead to improvements of packet loss probability, while it might bring longer delays. In addition, the service rate during the *deep-shadowing* status has a strong impact on the delay performance. This analysis sheds light on the design decisions for this type of systems. Future work will be on enhancing the end-to-end delay performance in such networks, while analyzing the trade-off between queue management policies and transport congestion control algorithms.

Acknowledgment

This project was funded by the EU Horizon 2020 research and innovation program, Drones4Safety-agreement No 861111, the Innovation Fund Denmark project Drones4Energy with project J. nr. 8057-00038A and by the Spanish Government (Ministerio de Economía y Competitividad, Fondo Europeo de Desarrollo Regional, MINECO-FEDER) by means of the project FIERCE: Future Internet Enabled Resilient smart CitiEs (RTI2018-093475-AI00).

References

[1] F. Rinaldi, H.-L. Maattanen, J. Torsner, S. Pizzi, S. Andreev, A. Iera, Y. Koucheryavy, and G. Araniti, "Non-terrestrial networks in 5g amp; beyond: A survey," *IEEE Access*, vol. 8, pp. 165 178–165 200, 2020.

[2] X. Lin, S. Cioni, G. Charbit, N. Chuberre, S. Hellsten, and J.-F. Boutillon, "On the path to 6g: Embracing the next wave of low earth orbit satellite access," *IEEE Communications Magazine*, vol. 59, no. 12, pp. 36–42, 2021.

[3] F. P. Fontan, M. Vazquez-Castro, C. E. Cabado, J. P. Garcia, and E. Kubista, "Statistical modeling of the lms channel," *IEEE Transactions on Vehicular Technology*, vol. 50, no. 6, pp. 1549–1567, 2001.

[4] N. J. Hernández Marcano, L. Diez, R. Agüero Calvo, and R. H. Jacobsen, "On the queuing delay of time-varying channels in low earth orbit satellite constellations," *IEEE Access*, vol. 9, 2021.

[5] A. Chen, C. Chang, and Y. Yao, "Performance evaluation of arq operations with obp and inter-satellite links: delay performance," in *IEEE 54th Vehicular Technology Conference Proceedings (VTC Fall 2001)*, vol. 4, 2001, pp. 2346–2350 vol.4.

[6] R. Hermenier, C. Kissling, and A. Donner, "A delay model for satellite constellation networks with inter-satellite links," in *2009 International Workshop on Satellite and Space Communications*, 2009, pp. 3–7.

[7] R. Prieto-Cerdeira, F. Perez-Fontan, P. Burzigotti, A. Bolea-Alamañac, and I. Sanchez-Lago, "Versatile two-state land mobile satellite channel model with first application to dvb-sh analysis," *International Journal of Satellite Communications and Networking*, vol. 28, no. 5-6, pp. 291–315, 2010. [Online]. Available: https://onlinelibrary.wiley.com/doi/abs/10.1002/sat.964

[8] D. Arndt, T. Heyn, J. König, A. Ihlow, A. Heuberger, R. Prieto-Cerdeira, and E. Eberlein, "Extended two-state narrowband lms propagation model for s-band," in *IEEE international Symposium on Broadband Multimedia Systems and Broadcasting*, 2012, pp. 1–6.

[9] L. Tan, Y. Liu, and J. Ma, "Analysis of queuing delay in optical space network on leo satellite constellations," *Optik*, vol. 125, no. 3, pp. 1154 – 1157, 2014.

[10] Y. Zhu, M. Sheng, J. Li, and R. Liu, "Performance analysis of intermittent satellite links with time-limited queuing model," *IEEE Communications Letters*, vol. 22, no. 11, pp. 2282–2285, 2018.

[11] U. Speidel and L. Qian, "Striking a balance between bufferbloat and tcp queue oscillation in satellite input buffers," in *2018 IEEE Global Communications Conference (GLOBECOM)*, 2018, pp. 1–6.

[12] M. Neuts, *Matrix-geometric Solutions in Stochastic Models: An Algorithmic Approach*. Johns Hopkins University Press, 1981.

[13] B. Hajek, "Birth-and-death processes on the integers with phases and general boundaries," *Journal of Applied Probability*, vol. 19, no. 3, p. 488–499, 1982.

[14] L. Diez and R. Agüero Calvo. (2022) Queuing LEO simulator. [Online]. Available: https://github.com/tlmat-unican/queuing-leo